Appl. Phys. B 90, 197–200 (2008)
DOI: 10.1007/s00340-007-2895-0

Applied Physics B
Lasers and Optics

J. KALKMAN
H.W. VAN KESTEREN✉

Relaxation effects and high sensitivity photoacoustic detection of NO_2 with a blue laser diode

Philips Research Eindhoven, High Tech Campus 34, 5656 AE Eindhoven, The Netherlands

Received: 14 September 2007 /
Revised version: 6 November 2007
Published online: 19 January 2008 •

ABSTRACT A detection limit of 200 ppt of NO_2 in N_2 at atmospheric pressure was obtained with a photoacoustic detector and a high power blue laser diode. This corresponds to a normalized noise (1σ) equivalent absorption coefficient of 2×10^{-9} cm^{-1}W/Hz$^{0.5}$. Measurements at different laser modulation frequencies showed no frequency dependence of the photoacoustic signal, indicating a relaxation time $\tau < 4$ μs. Mixing O_2 into the NO_2 containing gas results in a decrease of the photoacoustic signal. A simple model shows that this effect can be attributed to an increased vibrational-vibrational relaxation of NO_2 to O_2.

PACS 31.70.Hq; 34.50.Ez; 42.55.Px

1 Introduction

Nitrogen dioxide is a toxic gaseous compound that is among the NO_x combustion products of fossil fuel. It can be found at high concentrations in urban areas along roads. The accurate and easy measurement of NO_2 at ppb levels is of importance for environmental pollution monitoring and can be used to maintain a healthy living environment. Here we present the photoacoustic measurement of NO_2 with a blue laser diode. Photoacoustics is a well-established and sensitive detection technique based on the generation of sound waves due to the intermittent absorption of light and subsequent thermal energy release [1]. NO_2 is characterized by a broadband absorption in the visible part of the spectrum that has been the subject of intense research [2, 3]. In our experimental design the blue laser emits at a wavelength within the broad absorption band of NO_2. We study the feasibility of obtaining an NO_2 detection sensitivity in the ppt range with a simple photoacoustic set-up using a blue laser diode. Furthermore we present a new method for determining the energy relaxation time by studying the effect of the modulation frequency on the signal strength. The influence of the main constituents of air on the photoacoustic detection of NO_2 is discussed. The effect of O_2 on the photoacoustic signal generation is studied in more detail because of its influence on the energy transfer during photoacoustic detection of NO_2.

✉ Fax: +31-40-4746321, E-mail: hans.van.kesteren@philips.com

2 Experimental

We measure NO_2 using a photoacoustic detection system with a cell design similar to that in [4]. The acoustic resonator has a length of 100 mm (resonance frequency 1688 Hz for N_2) and a diameter of 3.8 mm; the buffer volumes have a length of 50 mm. A high power Nichia GaN diode laser with an emission wavelength of 444 nm is used as a light source. The diode laser is mounted on a Peltier cooled stage to keep the temperature stable during high power operation. The output power is square wave modulated by modulating the drive current between the laser threshold current and a maximum current. The modulation frequency is tuned to the fundamental longitudinal resonance frequency of the acoustic resonator. The laser light is collimated through the photoacoustic cell by an NA = 0.55 aspherical lens. We use a Knowles EK-3024 electret condenser microphone to detect the acoustic signal. The in-phase microphone signal is obtained using an analog lock-in amplifier set to a time constant of 1 s. In all experiments the NO_2 concentration is measured on-line as a reference using an NO_2 to NO molybdenum converter in combination with an Eco Physics CLD88p chemoluminescence detector.

For all photoacoustic NO_2 measurements the NO_2 concentration entering the photoacoustic cell is varied between 10 and 800 ppb by mixing a nitrogen flow (5N-pure, Air Products, at 200–1000 sccm) and a NO_2 containing flow (3.2 ppm NO_2 in N_2, Praxair, 0–100 sccm). From the main flow, a flow of 200 or 300 sccm is passed through the photoacoustic cell. The measurements are carried out at atmospheric pressure.

3 Results and discussion

To increase the optical power in the acoustic resonator the photoacoustic cell is operated in double-pass configuration with a planar mirror opposite of the laser diode. Figure 1 shows the measured in-phase photoacoustic signal versus the NO_2 concentration (determined with chemoluminescence). A linear dependence can be observed over the whole NO_2 concentration range. From the linear fit and the noise of the measurements at zero NO_2 concentration, a noise equivalent detection limit (1σ) of 200 ppt at a 1 s integration time was

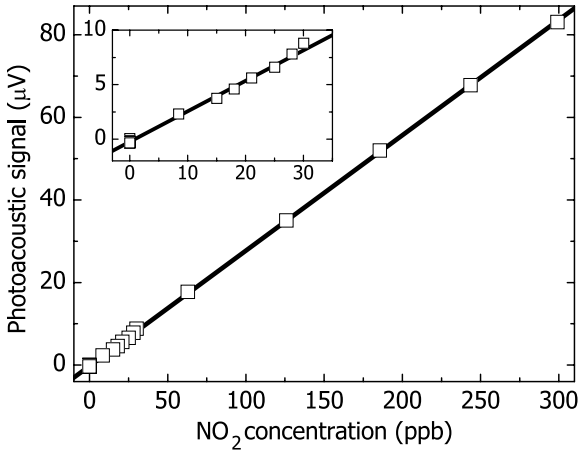

FIGURE 1 In-phase photoacoustic signal versus NO_2 concentration (determined with a reference). The *inset* more clearly shows the measurements at low NO_2 concentrations. A detection limit of 200 ppt was determined from this data

determined. The corresponding normalized noise equivalent absorption coefficient is calculated using the average power in the acoustic resonator (estimated from the average power in front and at the back of the resonator). The resulting average power is 333 mW, which in combination with the NO_2 absorption cross-section at 444 nm of 4×10^{-19} cm^2 [5] and the integration time of the lock-in amplifier (1 s), results in a noise equivalent absorption coefficient of 2×10^{-9} cm^{-1}W/Hz$^{0.5}$. This remarkable high NO_2 detection sensitivity is combined with a very simple and robust measurement set-up making our method very attractive compared to other measurement schemes such as described in [6].

The presence of interfering photoacoustic signals was studied for the three main atmospheric constituents: N_2, O_2 and H_2O. The experiments were carried out in a single pass configuration at a laser emission wavelength of 444 nm with an average power of 25 mW inside the resonator. First the acoustic resonance frequency was determined from the photoacoustic measurement of NO_2 for the various gas mixtures. Subsequent experiments without NO_2, at the appropriate modulation frequency for the applied gas mixture, showed no photoacoustic signals for concentrations up to 1.8 vol. % H_2O and 100 vol. % for N_2 and O_2.

Nitrogen and oxygen have no absorption lines in the 400–450 nm wavelength range according to the HITRAN database [7]. Water has a number of weak and narrow absorption lines in between 440–450 nm with absorption cross-sections in the $0.1–1.5 \times 10^{-25}$ cm^2 range [7, 8]. With the laser emission wavelength coinciding with one of these absorption lines, some signal interference can be expected to occur at high humidity levels during NO_2 detection in the low ppb range. Since NO_2 has such a broad absorption band photoacoustic interference can be avoided by an appropriate choice of the laser emission wavelength. For our experimental conditions, a 444 nm laser and a power of 25 mW, no measurable interference is expected. One of the few other gasses that might interfere is ozone, which has an absorption cross-section of 1×10^{-22} cm^2 at 444 nm [9]. Therefore, only for O_3 concentrations far above the MAC value of 60 ppb, interference will become significant.

The photoacoustic signal strength does not only depend on factors such as laser power, acoustic resonator quality factor, resonance frequency, microphone sensitivity, absorption strength and resonator volume [10], but also on the rate at which the energy from the photoexcited molecules decays. If the relaxation time τ is too long, the excited state population does not accurately follow the laser amplitude modulation resulting in a signal decrease. The signal decrease is given by [11]

$$\text{signal} \propto \frac{1}{\sqrt{1+(2\pi f_{\text{res}}\tau)^2}}\,, \tag{1}$$

with f_{res} the laser modulation frequency. Consequently, a too long relaxation time will result in reduced detection sensitivity.

To determine whether relaxation effects limit the detection limit of 200 ppt, we measure the photoacoustic signal strengths for various resonance frequencies. For this we use a multi-segment photoacoustic cell of which the length can be changed and we measure at the fundamental mode for each cell length (the middle segment, used for all these experiments, contains a fixed microphone). The photoacoustic cell is operated at ambient pressure under a flow of 300 sccm. The photoacoustic signal strength is determined from the slope of the signal versus concentration to eliminate any signal offset variation. We observed that for some acoustic resonator lengths, acoustic interference between the buffer volume and the resonator occurs that results in non-Lorentzian resonance shapes. As we correct the signal for resonator quality factor, we only use resonator lengths that match the buffer volume length and show Lorentzian acoustic line shapes (wavelength in buffer volume: $\lambda/4$, $3\lambda/4$, $5\lambda/4$, and $7\lambda/4$). The photoacoustic measurements at different frequencies are corrected for the following parameters:

- Acoustic cavity quality factor, as determined from the Lorentzian line shape of the signal versus frequency
- Frequency dependence of the microphone sensitivity, as determined from the sensitivity stated by the manufacturer (note that we use the same microphone for all experiments)
- NO_2 concentration, measured with chemoluminescence
- Optical power, measured for every modulation frequency
- Intrinsic $1/f$ photoacoustic frequency dependence

Consequently, any frequency dependence of the signal strength is only determined by the relaxation time as defined by (1). Figure 2 shows the corrected photoacoustic signal strength versus modulation frequency. The corrected photoacoustic signal strength is independent of modulation frequency up to a frequency of 15 kHz. The signal strength dependence according to (1) is also shown for a relaxation time of 4 μs and 40 μs. The data are best fitted by a straight line ($\tau = 0$), but simulations with relaxation times shorter than 4 μs also describe the data well; longer relaxation times are not in agreement with the data. We, therefore, conclude that our 200 ppt detection limit for NO_2 in N_2 is not restricted by relaxation effects as the relaxation time is much shorter than the modulation period of 600 μs.

The upper limit on the relaxation time is in agreement with the results of Hartland et al. [12] who show, using time-

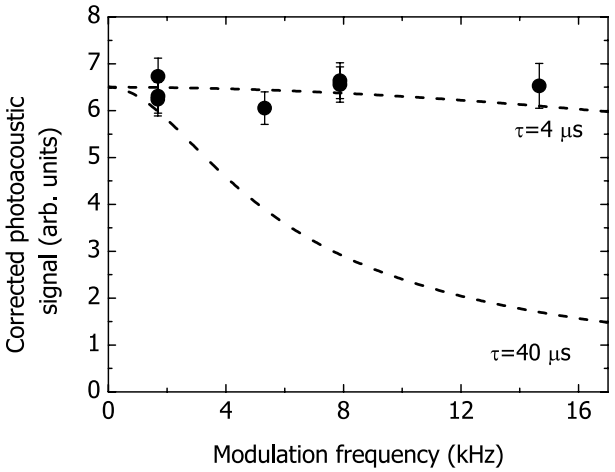

FIGURE 2 Corrected photoacoustic signal measured at different modulation frequencies. A simulation with (1) shows that the upper limit of the relaxation time is 4 μs. The result of (1) is also plotted for $\tau = 40\,\mu s$ for comparison

resolved Fourier transform infrared emission spectroscopy, a double exponential relaxation of NO_2 in N_2 after excitation at 475 nm. We fitted this curve and extrapolated the relaxation time to atmospheric pressures. The result was a relaxation time of $\sim 2\,\mu s$, which is in agreement with the 4 μs upper limit that we determined.

Relaxation effects due to mixing O_2 into the NO_2 containing gas mixture are investigated. Figure 3 shows the normalized photoacoustic signal for a varying O_2 concentration measured with the 100 mm cell (modulation frequency of 1688 Hz in N_2). The photoacoustic signal is corrected for dilution with O_2 and measured at the acoustic resonance frequency, which shifts with increasing O_2 concentration. The photoacoustic signal is decreased by 20% when 50 vol. % O_2 is mixed into the gas. A measurement with a photoacoustic cell with a length of 20 mm (resonance frequency of 7880 Hz in N_2) showed a signal decrease of the photoacoustic signal with O_2 concentration similar to that for the 100 mm cell, thereby confirming the high relaxation rate. For the detection of NO_2 in environmental air, in which the oxygen concentration is constant, the influence of O_2 on the photoacoustic signal strength will cause no problem.

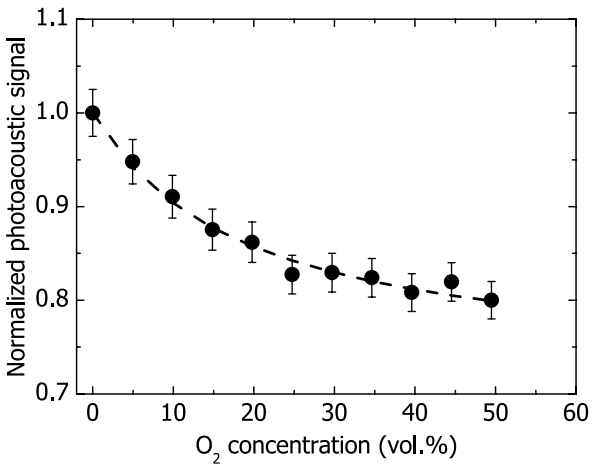

FIGURE 3 Normalized NO_2 photoacoustic signal vs. O_2 concentration and a fit to the data with the model of (2) (*dashed line*)

Figure 4 shows a schematic describing the excited state of NO_2 and its decay. NO_2 is excited to the $^2B_2$ state and its excitation energy is lost to photoacoustic signal generation by VT-relaxation of NO_2 in collisions with N_2 ($k_{N_2\text{-VT}}$) and O_2 ($k_{O_2\text{-VT}}$). Processes that do not lead to photoacoustic signal generation are described by VV-relaxation of NO_2 to these molecules ($k_{N_2\text{-VV}}$ and $k_{O_2\text{-VV}}$). The thus defined decay rates are decay rates averaged over energies from the excitation energy down to the ground state. Fluorescence decay is not included in this model since collisional deactivation is a much faster process at atmospheric pressure. No frequency dependence is included since we have shown that the relaxation rate is much faster than the modulation frequency of 1688 Hz. The generated photoacoustic signal as a function of oxygen concentration x is

$$\text{photoacoustic signal} \propto \frac{(1-x)+x\frac{k_{O_2\text{-VT}}}{k_{N_2\text{-VT}}}}{(1-x)\left(1+\frac{k_{N_2\text{-VV}}}{k_{N_2\text{-VT}}}\right)+x\left(\frac{k_{O_2\text{-VT}}}{k_{N_2\text{-VT}}}+\frac{k_{O_2\text{-VV}}}{k_{N_2\text{-VT}}}\right)}. \quad (2)$$

A fit of (2) to the data shows good agreement, but does not give a unique fit solution. Of the two-parameter fits, only a fit with $k_{N_2\text{-VV}}/k_{N_2\text{-VT}}$ set to zero shows good agreement to the data, as can be seen by the fit to the data in Fig. 3. This unique fit solution is $k_{O_2\text{-VT}}/k_{N_2\text{-VT}} = 5$ and $k_{O_2\text{-VV}}/k_{N_2\text{-VT}} = 1.5$.

As we excite NO_2 high into the $^2B_2$ state a whole manifold of energy levels is present for energies in excess of the $^2B_2$ threshold energy. Relaxation in this energy range is fast and is due to collisions with N_2 and O_2. At energies below the $^2B_2$ threshold energy a discrete set of energy levels from the $^2A_1$ state, defined by the vibrational energies ν_1, ν_2, and ν_3 of NO_2, can be found [12, 13]. The ν_3 vibrational energy level of $^2A_1$ is at 1617 cm^{-1}, which is very close to the vibrational energy of O_2 at 1556 cm^{-1}. We therefore expect some resonant energy transfer between NO_2 and O_2 in which a vibrational quantum in O_2 is excited. As excited O_2 decays very slowly (63^{-1} Hz [14]), this energy is essentially lost for the coherent photoacoustic signal generation. Consequently, we attribute the $k_{O_2\text{-VT}}/k_{N_2\text{-VT}}$ ratio to efficient VT-relaxation at high energies (above the $^2B_2$ threshold) whereas the $k_{O_2\text{-VV}}/k_{N_2\text{-VT}}$ ratio expresses VV-relaxation at low energies. The vibrational energy of N_2 at 2330 cm^{-1} is not resonant with the

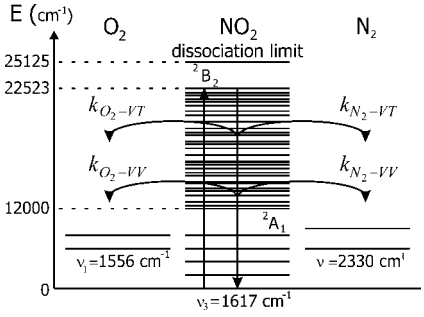

FIGURE 4 Energy diagram showing the relaxation of NO_2 to N_2 and O_2. The NO_2 is excited into the $^2B_2$ state and decays to the ground state via VT and VV relaxation to O_2 and N_2

NO_2 vibrational energy and will, therefore, not lead to much VV-relaxation, in agreement with our two-parameter fit with $k_{N_2\text{-VV}}/k_{N_2\text{-VT}}$ set to zero. Although the full dynamics of the NO_2 relaxation is very much simplified in this model we do think that it captures the basic relaxation dynamics. Photoacoustic measurements at varying excitation energies can be performed to further elucidate the photoacoustic decay mechanism of NO_2 in the presence of O_2.

4 Conclusions

We presented the high sensitivity photoacoustic detection of NO_2 in N_2 and showed that a detection limit of 200 ppt at a 1 s integration time is feasible with a high power blue diode laser. The relaxation time is short and does not affect the detection limit of the photoacoustic measurement. With an appropriate choice of the laser wavelength the NO_2 detection is free from interfering photoacoustic signals of N_2, O_2 and H_2O. We show a photoacoustic signal decrease when oxygen is mixed into the gas mixture and attribute this to an increased VV-relaxation due to oxygen.

ACKNOWLEDGEMENTS The authors are grateful for fruitful discussions with Dr. Frans Harren of the Radboud University Nijmegen.

REFERENCES

1 A. Miklós, P. Hess, Rev. Sci. Instrum. **72**, 1937 (2001)
2 G.D. Gillispie, A.U. Khan, A.C. Wahl, R.P. Hosteny, M. Krauss, J. Chem. Phys. **63**, 3425 (1975)
3 G.D. Gillispie, A.U. Khan, J. Chem. Phys. **65**, 1624 (1976)
4 F.G.C. Bijnen, J. Reuss, F.J.M. Harren, Rev. Sci. Instrum. **67**, 2914 (1996)
5 A.C. Vandaele, C. Hermans, P.C. Simon, M. Carleer, R. Colin, S. Fally, M.F. Merienne, A. Jenouvrier, B. Coquart, J. Quant. Spectrosc. Radiat. Transf. **59**, 171 (1998)
6 V.L. Kasyutich, P.A. Martin, R.J. Holdsworth, Meas. Sci. Technol. **17**, 923 (2006)
7 L.S. Rothman, D. Jacquemart, A. Barbe, D.C. Benner, M. Birk, L.R. Brown, M.R. Carleer, C.J. Chakerian, K.V. Chance, V. Dana, V.M. Devi, J.-M. Flaud, R.R. Gamache, A. Goldman, J.-M. Hartmann, K.W. Jucks, A. Maki, J.-Y. Mandin, S.T. Massie, J. Orphal, A. Perrin, C.P. Rinsland, M.A.H. Smith, J. Tennyson, R.N. Tolchenov, R.A. Toth, J. Vander Auwera, P. Varanasi, G. Wagner, J. Quant. Spectrosc. Radiat. Transf. **96**, 139 (2005)
8 P.-F. Coheur S. Fally, M. Carleer, C. Clerbaux, R. Colin, A. Jenouvrier, M.-F. Mérienne, C. Hermans, A.-C. Vandaele, J. Quant. Spectrosc. Radiat. Transf. **74**, 493 (2002)
9 J.P. Burrows, A. Richter, A. Dehn, B. Deters, S. Himmelman, S. Voigt, J. Orphal, J. Quant. Spectrosc. Radiat. Transf. **61**, 509 (1999)
10 W. Demtröder, *Laser Spectroscopy* (Springer, Berlin, 2002)
11 L. Rosengren, Infrared Phys. **13**, 109 (1973)
12 G.V. Hartland, D. Qin, H.-L. Dai, C. Chen, J. Chem. Phys. **107**, 2890 (1997)
13 A. Delon, R. Jost, J. Chem. Phys. **95**, 5686 (1991)
14 H.E. Bass, H.-J. Bauer, Appl. Opt. **12**, 1506 (1973)